ALGORITHM THEORETICAL BASIS DOCUMENT (ATBD):

EDDY-COVARIANCE DATA PRODUCTS COMPOSITE

PREPARED BY	ORGANIZATION	DATE
Stefan Metzger	NEON	2017-12-05
Hongyan Luo	NEON	2017-12-04
Ke Xu	NEON	2017-07-27
David Durden	NEON	2017-06-21
Natchaya Pingintha-Durden	NEON	2017-06-15

APPROVALS	ORGANIZATION	APPROVAL DATE

RELEASED BY	ORGANIZATION	RELEASE DATE

See configuration management system for approval history.

Change Record

REVISION	DATE	ECO #	DESCRIPTION OF CHANGE
A	06/21/2017	ECO-XXXXX	Initial release

TABLE OF CONTENTS

LIST OF TABLES AND FIGURES

1   DESCRIPTION

The National Ecological Observatory Network (NEON) seeks to address grand challenges in continental-scale ecology through extensive observational infrastructure across the U.S. One core element are eddy-covariance (EC) flux measurements of ecologically-relevant energy, water, and trace gas fluxes.

1.1   Purpose

This document describes the theoretical background and entire algorithmic process for calculating the general statistics of state variables including means, minimum values, maximum values, variances, uncertainty and data quality of outputs from EC turbulent and storage exchange sensors.

1.2   Scope

The theoretical background and entire algorithmic process used to derive Level 1-4 (dp01-dp04) data products (DP) from pre-conditioned Level 0 raw data (dp0p) for all eddy-covariance data product is described in this document. The eddy-covariance system primarily consists of two major subsystems, eddy-covariance turbulent exchange subsystem (ECTE) and eddy-covariance storage exchange subsystem (ECSE). This ATBD first introduces related documents, acronyms and conventions (Sect. 2). Throughout Sects. 3–5, (i) all reported variables and input variables are identified, (ii) theoretical background is provided, (iii) explicit algorithm descriptions are given, and (iv) error propagation algorithms are provided that enable the calculation of uncertainty budgets for each reported variable. The command, control, and configuration (C3) documents for ECTE [AD01] and ECSE [AD02] include a discussion of all necessary requirements for operational control parameters, conditions/constraints, set points, and any necessary error handling for the physical implementation of the subsystems. Prior to the scientific processing described in the present document, all Level 0 raw data are pre-conditioned as detailed in AD[03] and AD[TBD].

2   RELATED DOCUMENTS, ACRONYMS AND VARIABLE NOMENCLATURE

2.1   Applicable Documents

AD[01]	NEON.DOC.000465 Eddy-covariance turbulent exchange subsystem C^3
AD[02]	NEON.DOC.000465 Eddy-covariance storage exchange subsystem C^3
AD[03]	NEON.DOC.000807 NEON Algorithm Theoretical Basis Document (ATBD) – Eddy Covariance Turbulent Exchange Subsystem Level 0 to Level 0 prime
AD[04]	NEON.DOC.000573 FIU plan for airshed QA/QC development
AD[05]	NEON.DOC.001113 Quality Flags and Quality Metrics for TIS Data Products ATBD
AD[06]	NEON.DOC.011081 ATBD QA/QC plausibility testing
AD[07]	NEON.DOC.001069 Preprocessing for TIS Level 1 Data Products
AD[08]	NEON.DOC.002651 Data Product Naming Convention

AD[09]	NEON.DOC.011081 ATBD QA/QC plausibility testing
AD[10]	NEON.DOC.001069 Preprocessing for TIS Level 1 Data Products

2.2   Reference Documents

RD[01]	NEON.DOC.000008 NEON Acronym List
RD[02]	NEON.DOC.000243 NEON Glossary of Terms

3   DATA PRODUCT DESCRIPTION

3.1   Variables Reported

The eddy-covariance related DPs provided by the algorithms documented in this ATBD are listed Table 1. They are provided in the form of HDF5 files (Sect. 3.2), including a description of all file structure and objects. Each Data Product encompasses several sub-products, as detailed in Sect. 5.2.1.4. The units of the individual sub-products are provided in the HDF5 file.

This document aims to provide all algorithmic processing and subsequent data products listed in Table 1. Thus, this document will grow as more data products become available. Currently available data products for this release are dp01 DPs of:

- 3D Wind Speed, Direction and Sonic Temperature
- 3D Wind Attitude and Motion Reference
- CO_2 Concentration - Turbulent
- H_2O Concentration - Turbulent
- CO_2 Concentration - Storage
- H_2O Concentration - Storage

Table 1. List of variables reported.

Instrument system	Product level	Description	Temporal resolution	Data Product Number	HDF5 Data Product ID Name
Re-ingested	dp01 statistics	Single Aspirated Air Temperature		NEON.DP1.00002	tempAirLvl
		Triple Aspirated Air Temperature		NEON.DP1.00003	tempAirTop
		Soil Heat Flux Plate		NEON.DP1.00040	fluxHeatSoil

Instrument system	Product level	Description	Temporal resolution	Data Product Number	HDF5 Data Product ID Name
		Shortwave and Longwave Radiation		NEON.DP1.00023	radiNet
EC turbulence	dp01 statistics	3D Wind Speed, Direction and Sonic Temperature	1 min, 30 min	NEON.DP1.00007	soni
		3D Wind Attitude and Motion Reference	1 min, 30 min	NEON.DP1.00010	soniAmrs
		CO_2 Concentration - Turbulent	1 min, 30 min	NEON.DP1.00034	irgaCo2
		H_2O Concentration - Turbulent	1 min, 30 min	NEON.DP1.00035	irgaH2o
EC profile	dp01 statistics	CO_2 Concentration - Storage	2 min, 30 min	NEON.DP1.00099	co2Stro
		H_2O Concentration - Storage	2 min, 30 min	NEON.DP1.00100	h2oStor
		Atmospheric CO_2 Isotopes	9 min, 30 min	NEON.DP1.00036	isoCo2
		Atmospheric H_2O isotopes	9 min, 30 min	NEON.DP1.00037	isoH2o
EC profile	dp02 time-interpolated	Temperature rate of change	30 min	NEON.DP2.xxxxx	tempStor
		CO_2 concentration rate of change	30 min	NEON.DP2.00008	co2Stor
		H_2O concentration rate of change	30 min	NEON.DP2.00009	h2oStor
EC profile	dp03 space-interpolated	Temperature rate of change profile	30 min	NEON.DP3.00008	tempStor
		CO_2 concentration rate of change profile	30 min	NEON.DP3.00009	co2Stor
		H_2O concentration rate of change profile	30 min	NEON.DP3.00010	h2oStor
	dp04 fluxes	Sensible heat flux	30 min	NEON.DP4.00002	fluxHeat

Instrument system	Product level	Description	Temporal resolution	Data Product Number	HDF5 Data Product ID Name
EC profile + turbulence combined		Momentum Flux	30 min	NEON.DP4.00007	fluxMome
		Latent heat flux	30 min	NEON.DP4.00137	fluxH2o
		Carbon dioxide flux	30 min	NEON.DP4.00067	fluxCo2
		Footprint characteristics	30 min	NEON.DP4.xxxxx	foot

3.2 HDF5 Representation

Hierarchical Data Format (HDF), currently distributed as HDF5, provides a file format with high compressibility, fast efficient reading and writing capabilities, directory-style files, and metadata attachment. The HDF5 file formats allow us to package various data sets into a single file with built-in structure for managing both data and metadata. The current NEON processing design utilizing the eddy4R package within a Docker framework employs HDF5 files for input/output operations. The NEON HDF5 file structure was developed following the data product naming convention provided in AD[08], where portions of the naming convention as described below were selected to develop the hierarchical structure of the HDF5 file (Figure 1):

NEON.DOM.SITE.DPL.PRNUM.REV.TERMS.HOR.VER.TMI

WHERE:

NEON=NEON

DOM=DOMAIN, e.g. D10

SITE=SITE, e.g. STER

DPL=DATA PRODUCT LEVEL, e.g. DP1

PRNUM = PRODUCT NUMBER =>5 digit number. Set in data products catalog.

TIS = 00000-09999

REV = REVISION, e.g. 001.

TERMS=From NEON's controlled list of terms. Index is unique across products.

HOR = HORIZONTAL INDEX. Semi-controlled; AIS and TIS use different rules.

Examples: Tower=000, HUT=700.

VER = VERTICAL INDEX. Semi-controlled; AIS and TIS use different rules.

Examples: Ground level=000, second tower level=020.

TMI=TEMPORAL INDEX. Examples: 001=1 minute, 030=30 minute, 999=irregular intervals.
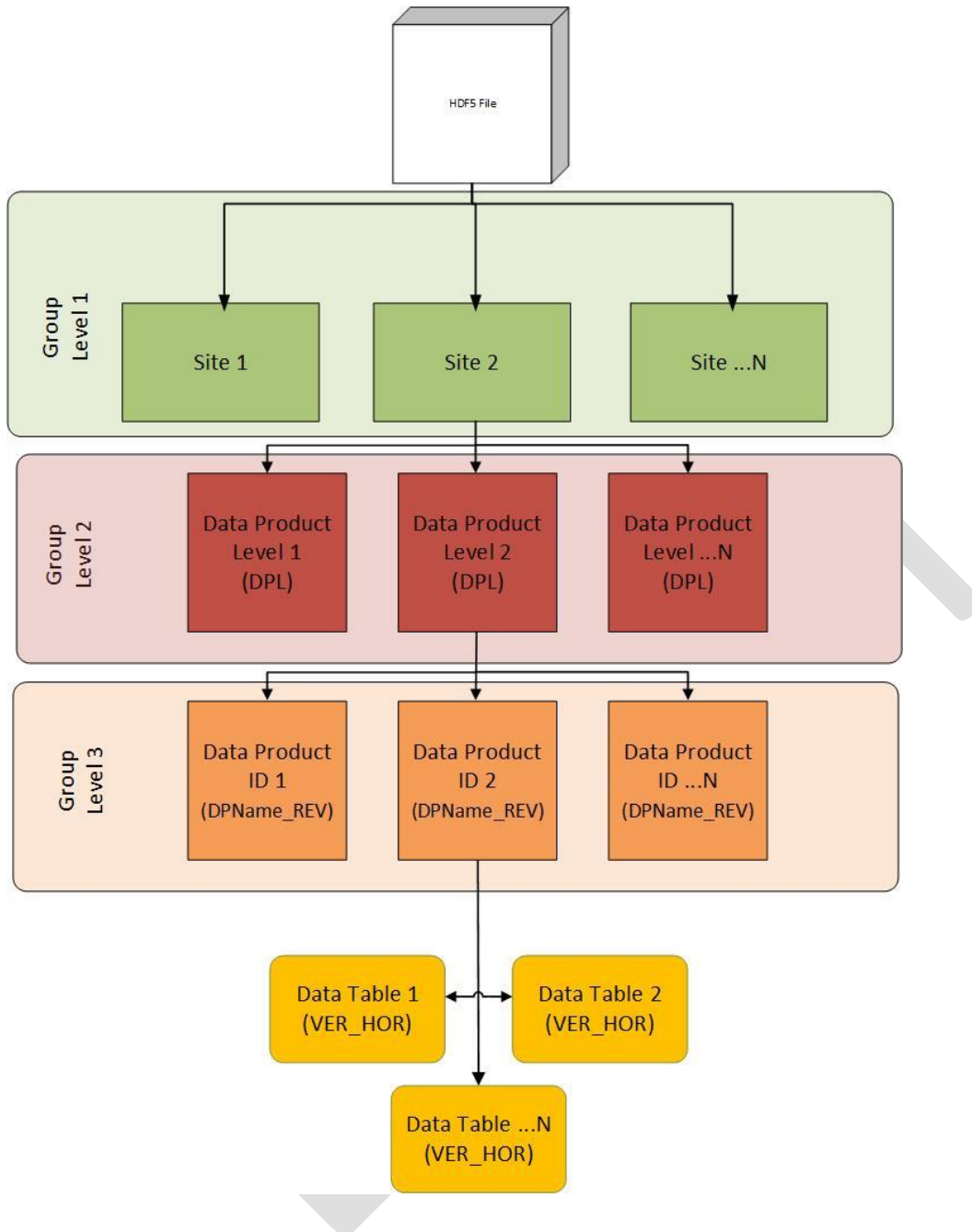
Figure 1. Diagram depicting the NEON HDF5 file structure following the NEON DP naming convention. Note that PRNUM is replaced by the DPName associated with that PRNUM.

One departure from the DP naming convention is the use of the data product name (DPName, e.g. irga) in place of PRNUM in the Data Product ID group level, this change was made to improve readability. At

the top level of the provided hdf5 file a readme and object description (objDesc) are provided to explain the contents of the file.

3.3   Input Dependencies

Below Table 2 - Table 7 detail the Eddy-covariance turbulent exchange (ECTE) related dp0p DPs used to produce dp01 DPs in this ATBD.

Table 2. List of soni-related dp0p DPs that are ingested in this ATBD.

dp0p Description	dp0p Term Name	Sample Frequency	Units
Measured along-axis wind speed (u_m)	veloXaxs	20 Hz	ms^{-1}
Measured cross-axis wind speed (v_m)	veloYaxs	20 Hz	ms^{-1}
Measured vertical-axis wind speed (w_m)	veloZaxs	20 Hz	ms^{-1}
Measured speed of sound (c_m)	veloSoni	20 Hz	ms^{-1}
Sonic temperature (T_{SONIC})	tempSoni	20 Hz	K
Sample count	idx	20 Hz	NA
Sensor error flag ($QF_{SONIC,o1}$: Sensor unresponsive)	qfSoniUnrs	20 Hz	NA
Sensor error flag ($QF_{SONIC,o2}$: No data available)	qfSoniData	20 Hz	NA
Sensor error flag ($QF_{SONIC,o3}$: Sensor trigger source lost)	qfSoniTrig	20 Hz	NA
Sensor error flag ($QF_{SONIC,o4}$: SDM communications error)	qfSoniComm	20 Hz	NA
Sensor error flag ($QF_{SONIC,o5}$: Wrong embedded sensor code)	qfSoniCode	20 Hz	NA
Sensor signal flag ($QF_{SONIC,s1}$: Axes T_{SONIC} difference > 4 K)	qfSoniTemp	20 Hz	NA
Sensor signal flag ($QF_{SONIC,s2}$: Poor signal lock)	qfSoniSgnlPoor	20 Hz	NA
Sensor signal flag ($QF_{SONIC,s3}$: High signal amplitude)	qfSoniSgnlHigh	20 Hz	NA
Sensor signal flag ($QF_{SONIC,s4}$: Low signal amplitude)	qfSoniSgnlLow	20 Hz	NA

Table 3. List of soniAmrs-related dp0p DPs that are ingested in this ATBD.

dp0p DP	dp0p Term Name	Sample Frequency	Units
Measured along-axis acceleration ($acc_{x,m}$)	accXaxs	40 Hz	$m\ s^{-2}$
Measured cross-axis acceleration ($acc_{y,m}$)	accYaxs	40 Hz	$m\ s^{-2}$
Measured vertical-axis acceleration ($acc_{z,m}$)	accZaxs	40 Hz	$m\ s^{-2}$

dp0p DP	dp0p Term Name	Sample Frequency	Units
Along-axis free acceleration	accXaxsDiff	40 Hz	m s^{-2}, positive forward
Cross-axis free acceleration	accYaxsDiff	40 Hz	m s^{-2}, positive left
Vertical-axis free acceleration	accZaxsDiff	40 Hz	m s^{-2}, positive up
Pitch rate	avelYaxs	40 Hz	rad s^{-1}
Roll rate	avelXaxs	40 Hz	rad s^{-1}
Yaw rate	avelZaxs	40 Hz	rad s^{-1}
Measured pitch angle (θ_m)	angYaxs	40 Hz	rad
Measured roll angle (ϕ_m)	angXaxs	40 Hz	rad
Yaw angle (ψ)	angZaxs	40 Hz	rad
Index value	idx	40 Hz	NA
Sensor signal flag: Selftest	qfAmrsVal	40 Hz	NA
Sensor signal flag: Filter Valid	qfAmrsFilt	40 Hz	NA
Sensor signal flag: NoVelocityUpdate status	qfAmrsVelo	40 Hz	NA
Sensor signal flag: Clipping indication	qfAmrsRng	40 Hz	NA

Table 4. List of irga-related dp0p DPs that are ingested in this ATBD.

dp0p DP	dp0p Term Name	Sample Frequency	Units
Cell temperature in (at sensor head inlet)	tempIn	20 Hz	K
Cell temperature out (at sensor head inlet)	tempOut	20 Hz	K
Cell temperature (weighted average of head inlet and outlet temperature)	tempMean	20 Hz	K
Block temperature	tempRefe	20 Hz	K
Ambient pressure (LI–7550 box pressure)	presAtm	20 Hz	Pa
Head pressure (differential pressure head-box)	presDiff	20 Hz	Pa
Total pressure (LI–7550 box pressure + head pressure)	presSum	20 Hz	Pa
H$_2$O sample power	powrH2oSamp	20 Hz	W
H$_2$O reference power	powrH2oRefe	20 Hz	W
H$_2$O raw absorptance	asrpH2o	20 Hz	-
H$_2$O molar density	densMoleH2o	20 Hz	mol m^{-3}
H$_2$O mixing ratio (dry mole fraction)	rtioMoleDryH2o	20 Hz	mol mol^{-1}
CO$_2$ sample power	powrCo2Samp	20 Hz	W
CO$_2$ reference power	powrCo2Refe	20 Hz	W
CO$_2$ raw absorptance	asrpCo2	20 Hz	-
CO$_2$ molar density	densMoleCo2	20 Hz	mol m^{-3}
CO$_2$ mixing ratio (dry mole fraction)	rtioMoleDryCo2	20 Hz	mol mol^{-1}

dp0p DP	dp0p Term Name	Sample Frequency	Units
Sequence number	idx	20 Hz	NA
LI-7200 diagnostic value 2 (sync clocks)	diag02	20 Hz	NA
LI-7200 cooler voltage	potCool	20 Hz	V
CO_2 signal strength	ssiCo2	20 Hz	-
H_2O signal strength	ssiH2o	20 Hz	-
Sensor flag (f_{L01}: Head detect)	qfIrgaHead	20 Hz	NA
Sensor flag (f_{L02}: Outlet temperature)	qfIrgaTempOut	20 Hz	NA
Sensor flag (f_{L03}: Inlet temperature)	qfIrgaTempIn	20 Hz	NA
Sensor flag (f_{L04}: Aux input)	qfIrgaAux	20 Hz	NA
Sensor flag (f_{L05}: Differential pressure)	qfIrgaPres	20 Hz	NA
Sensor flag (f_{L06}: Chopper)	qfIrgaChop	20 Hz	NA
Sensor flag (f_{L07}: Detector)	qfIrgaDetc	20 Hz	NA
Sensor flag (f_{L08}: PLL)	qfIrgaPll	20 Hz	NA
Sensor flag (f_{L09}: Sync)	qfIrgaSync	20 Hz	NA
Sensor flag (f_{L10}: AGC)	qfIrgaAgc	20 Hz	-

Table 5. List of irgaMfcSamp-related dp0p DPs that are ingested in this ATBD.

dp0p DP	dp0p Term Name	Data Format	Units
Sampling mass flow rate set point	frtSet00	20 Hz	m3 s-1
Sampling mass flow rate	frt00	20 Hz	m3 s-1
Sampling volumetric flow rate	frt	20 Hz	m3 s-1
Sampling gas pressure	presAtm	20 Hz	Pa
Sampling gas temperature	temp	20 Hz	K

Table 6. List of co2Stor-related dp0p DPs that are ingested in this ATBD.

dp0p DP	dp0p Term Name	Data Format	Units
Sampling mass flow rate	frt00	1 Hz	m3 s-1
Sampling gas pressure	pres	1 Hz	Pa
CO_2 mixing ratio (dry mole fraction)	rtioMoleDryCo2	1 Hz	$mol\ mol^{-1}$
CO_2 mixing ratio (wet mole fraction)	rtioMoleWetCo2	1 Hz	$mol\ mol^{-1}$
Sampling gas temperature	temp	1 Hz	K
CO_2 mixing ratio (dry mole fraction)	rtioMoleDryCo2	1 Hz	$mol\ mol^{-1}$

Table 7. List of h2oStor-related dp0p DPs that are ingested in this ATBD.

dp0p DP	dp0p Term Name	Data Format	Units
Sampling mass flow rate	frt00	1 Hz	m3 s-1
Sampling gas pressure	pres	1 Hz	Pa

dp0p DP	dp0p Term Name	Data Format	Units
H$_2$O mixing ratio (dry mole fraction)	rtioMoleDryH2o	1 Hz	mol mol^{-1}
H$_2$O mixing ratio (wet mole fraction)	rtioMoleWetH2o	1 Hz	mol mol^{-1}
Sampling gas temperature	temp	1 Hz	K

In addition, standard NEON TIS sensor plausibility tests are applied at native temporal resolution to the dp0p DPs listed above. The corresponding pass/fail flags per Table 8 are generated for each test according to AD[09]. (Note. We will not be carrying out the "gap test" or "null test" since the regularization is being applied according to AD[10]).

Table 8. Plausibility quality flags to be applied to all dp0p DPs

Flag	Term modifier	Description
QF_{Cal}	qfCal	Quality flag for the Invalid Calibration test
QF_{Pers}	qfPers	Quality flag for the Persistence test
QF_{Rng}	qfRng	Quality flag for the Range test
QF_{Step}	qfStep	Quality flag for the Step test

The flags are applied to all dp0p DP following a uniform naming convention, whereby the dp0p DP term name is augmented with the plausibility test flag term modifier. For example, the quality flag for the step test for measured along-axis wind speed will be "qfStepVeloXaxs".

Lastly, solenoid flags that indicate validation periods are outlined in Table 7. These data do not have quality flag information associated with the measurements.

Table 9. irgaSndValiNema -related dp0p DPs that are ingested in this ATBD.

dp0p DP	dp0p Term Name	Sample Frequency	Units
Validation gas 1-5 status NEMA enclosure	qfGas01 – qfGas05	0.2 Hz	NA

3.4 Product Instances

Each NEON site with terrestrial infrastructure will produce an instance of the reported variables in Table 1.

3.5   Temporal Resolution and Extent

The temporal resolution/extent of all reported variables in ECTE instrument system under Table 1 is 1 min and 30 min. The temporal resolution of most input variables in ECTE instrument system in Table 2 – Table 5 is 0.05 s (20 Hz) (design described in AD[01]), with exception of the mean soniAmrs variables collected at measurement frequency of 0.025 s (40 Hz). The temporal extent of all input variables is 0.5 h, i.e. a data set of 0.5 h duration shall be considered for each implementation of the presented algorithms.

The temporal resolution/extent of dp01 CO_2 and H_2O concentration data products under Table 1 is 2 min (or 9 min) and 30 min for ECSE instrument system. The temporal resolution of all input variables in Table 6–Table 7 is 1 s (1 Hz). The temporal extent of all input variables is 1 day, i.e. a data set of 1 day duration shall be considered for each implementation of the presented algorithms.

3.6   Spatial Resolution and Extent

The input variables used in this ATBD are measured at a single position in space. Consequently both, input variables and reported variables are not spatially resolved. The 3D boom accelerations (acc_x, acc_y, acc_z) are point measurements. The spatial extent (path length) of all remaining variables is ≈10 cm (AD[03]). The spatial representativeness of the means, variances and covariances reported in this ATBD is a function of several factors such as measurement height $d_{z,m}$, displacement height $d_{z,d}$, wind speed and direction, atmospheric stability and surface roughness. From dispersion modeling (e.g., Schmid, 1994; Vesala et al., 2008) it is found that ≈10 ($d_{z,m}-d_{z,d}$) < $d_{x,FP90}$ < 100 ($d_{z,m}-d_{z,d}$), where $d_{x,FP90}$ is the cross-wind integrated upwind extent from within which 90% of a measured flux value is sourced. The spatial representativeness for each observation of the reported variables will be quantified during the implementation of AD[04].

3.7   Overall algorithmic implementation

NEON utilizes the eddy4R-Docker EC data processing environment (Metzger et al., 2017) to routinely perform the calculations outlined in the following sections. eddy4R-Docker relies on the eddy4R family of open-source packages for EC raw data processing, analyses and modeling in the R Language for Statistical Computing (R Core Team, 2016), wrapped into a Docker filesystem that contains only the minimal context needed to run.

To perform a defined series of processing steps, the eddy4R-Docker image is called with a instruction set, resulting in a running instance called Docker container (Figure 2). Through this mechanism, an arbitrary number of eddy4R-Docker containers can be run simultaneously performing identical or different services depending on the workflow file. This provides an ideal framework for scaled deployment using e.g. high-throughput compute architectures, cloud-based services etc.
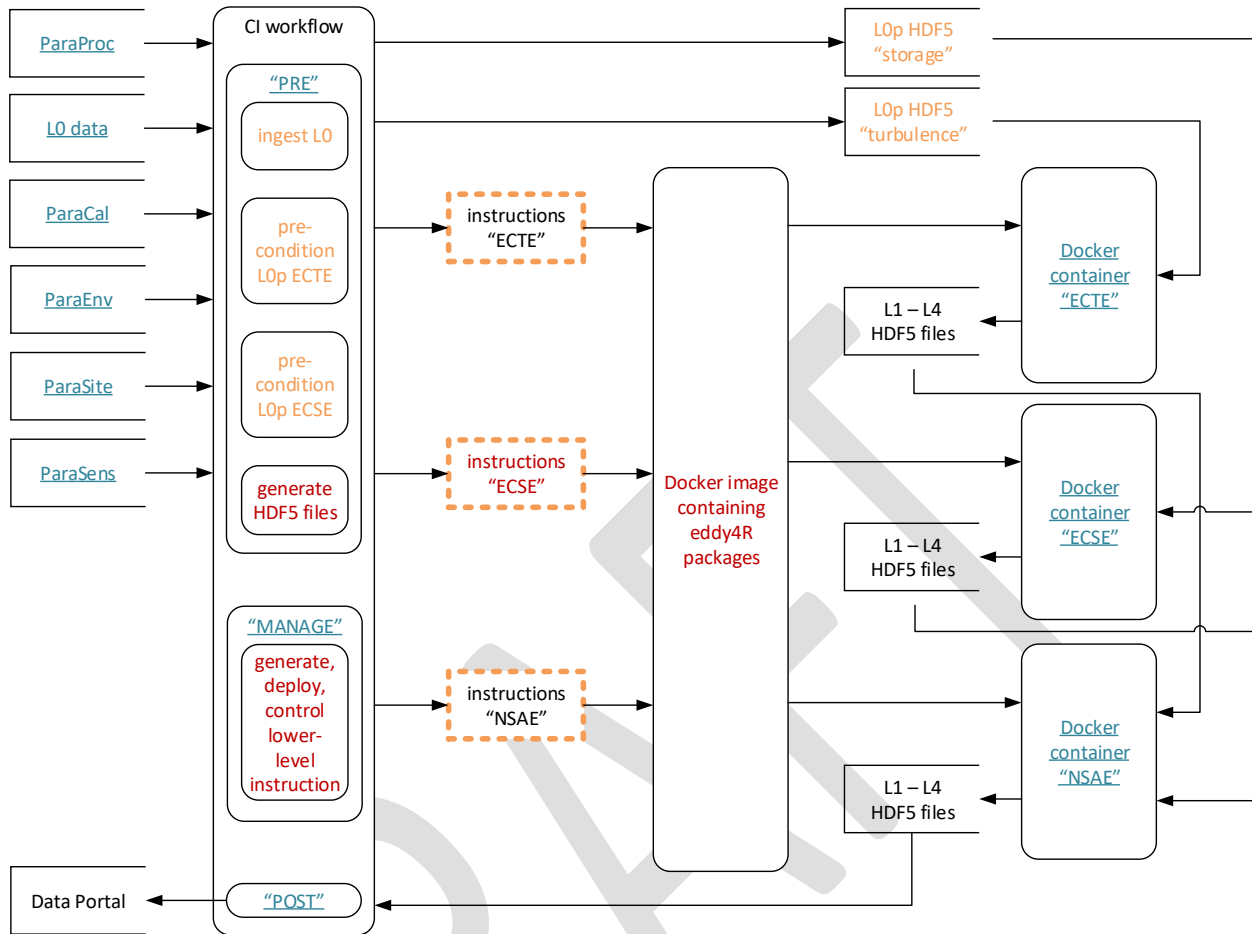
Figure 2. NEON's eddy4R-Docker EC processing framework. Individual components are described in the text.

The overall processing framework begins with ingesting information from various data sources on a site-by-site basis (Figure 2 top left). This includes EC raw data (Level 0, or L0 data) alongside contextual information on measurement site (ParaSite), environment (ParaEnv), sensor (ParaSens), calibration (ParaCal), as well as processing parameters (ParaProc). Next, the raw data is preconditioned and all information is hierarchically combined into a compact and easily transferable HDF5 file (Figure 2 panel "CI workflow"). Each file contains the calibrated raw data (L0 prime, or L0p) and metadata for one site and one day, either for EC turbulent exchange or storage exchange. Together with the corresponding turbulence (ECTE), storage (ECSE) or net surface-atmosphere exchange (NSAE) instruction sets the HDF5 L0p data file is passed to the eddy4R-Docker image, where a running Docker container is spawned that performs the specified computations (Figure 2 top right). The resulting higher-level data products (Level 1 – Level 4, or dp01-dp04) are collected and, together with all contextual information, are combined into

a daily dp01-dp04 HDF5 data file that is served on the data portal (Figure 2 bottom left). In addition to the daily output files, monthly concatenated files are also available for download from the NEON data portal.

The eddy4R-Docker EC data processing environment is publicly available and extensible, and continuously solicits community input through a Development and Systems Operations approach (Metzger et al., 2017).

4 SCIENTIFIC CONTEXT

The intention of NEON EC measurements is to determine the surface-air exchange of momentum, heat, water vapor and CO_2 from measurements of the wind vector, temperature, and scalar concentration.

5 TURBULENT EXCHANGE

The calculation of eddy-covariance momentum, heat, water vapor and carbon dioxide fluxes provides higher-level DPs with ecological relevance. These DPs are used for constraining, calibrating and validating process-based models (e.g., Rastetter et al., 2010). This shall enable the detection of continental scale ecological change and the forecasting of its impacts.

5.1 Theory of Measurement

The exchange of momentum, heat, water vapor, CO_2 and other scalars between the earth's surface and the atmosphere is mainly governed by turbulent transport. Buoyancy as well as shear stress result in a turbulent wind field for most of the day (e.g., Stull, 1988). The eddy-covariance (EC) technique measures the properties of the turbulent wind field directly. This makes it the least invasive method currently available for direct and continuous observations of the surface-air exchange. The technique is based on the concept of mass conservation and makes use of the Reynolds decomposition (isolation of mean and fluctuating part) of relevant terms in the Navier-Stokes equation (e.g., Foken, 2008; Stull, 1988). With several restrictions (AD[04]) the net flux F into or out of an ecosystem can be expressed as (e.g., Loescher et al., 2006);

$$F = \underbrace{\int_0^{d_{z,m}} \frac{\partial \bar{X}}{\partial t} dz}_{\text{I}} + \underbrace{\int_0^{d_{z,m}} \frac{\partial \overline{u'X'}}{\partial x} dz}_{\text{II}} + \underbrace{\int_0^{d_{z,m}} \frac{\partial \overline{v'X'}}{\partial y} dz}_{\text{III}} + \underbrace{\int_0^{d_{z,m}} \frac{\partial \overline{w'X'}}{\partial z} dz}_{\text{IV}}$$

$$+ \underbrace{\int_0^{d_{z,m}} \frac{\partial \bar{u}\bar{X}}{\partial x} dz}_{\text{V}} + \underbrace{\int_0^{d_{z,m}} \frac{\partial \bar{v}\bar{X}}{\partial y} dz}_{\text{VI}} + \underbrace{\int_0^{d_{z,m}} \frac{\partial \bar{w}\bar{X}}{\partial z} dz}_{\text{VII}},$$

$$(1)$$

with overbars denoting means, and primes denoting deviations from the mean. Here, X is a scalar quantity such as H_2O or CO_2 mixing ratios; u, v and w are along-, cross-, and vertical wind speeds with respect to the Cartesian coordinates x, y, and z; t is time, and $d_{z,m}$ is the measurement height. Term I in Eq. (1) represents the positive or negative rate of change of Y in the vertical column below the sensor, equivalent to storage. Terms II–IV represent the turbulent flux divergence, and terms V–VII represent advection through the layer between the surface and sensor. If the conditions at the measurement site fulfill several assumptions (details provided in AD[04]), terms I–III and V–VII cancel from Eq. (1), and term IV can be further simplified to;

$$F = \overline{w'X'}. \tag{2}$$

That is, in this case the net flux into or out of an ecosystem can be expressed as the covariance between the vertical wind and the scalar, which can be computed from EC-TES measurements alone. Whether or not this reduction of Eq. (1) is valid will be assessed in a series of tests during the implementation of AD[01]. Wherever possible, auxiliary measurements will be used to re-substitute non-negligible terms in Eq. (2), e.g. the storage term I (AD[04]).

5.2   Data Analysis

5.2.1   Theory of Algorithm

The subject of this ATBD is the mathematical derivation of statistical quantities in Eq. (1). These quantities are used to (i) express the net flux according to Eq. (2), and (ii) quantify the fulfillment of assumptions on the site conditions during the implementation of AD[05].

5.2.1.1   De-spiking

The time series signal despiking algorithm by (Brock, 1986) is used, including the additional threshold by (Starkenburg et al., 2016). This study concluded that the median filter approach resulted in robust despiking results with little to no misclassification of spikes.

5.2.1.2   Lag-correction

Application of Eq. (1) requires that the instantaneous quantities X_i and Y_i are measured at the same place and at the same time, which usually is not possible. Consequently, before applying Eq. (1), the recorded time series must be adjusted by a certain time lag to ensure spatiotemporal coincidence. The delay between the two time series is mainly caused by differences in electronic signal treatment, spatial separation between wind and scalar sensors, and air travel through the tubes in closed-path gas analyzers. Assuming joint stationarity, the lag time l can be estimated for each averaging interval by performing a cross correlation analysis between the quantities of interest;

$$\text{abs}\left(\frac{\overline{X\prime(t)\cdot Y\prime(t+l)}}{\overline{X\prime}\cdot\overline{Y\prime}}\right) \to \max, \tag{3}$$

for samples collected at times t and $t+l$. This is equivalent to comparing the correlations between the quantities lagged by different delays (Figure 3). The time lag that results in the highest correlation is selected. However, when correlations are small this procedure can result in ambiguous lag times. Hence, high-pass filtering and pre-defining the maximum size of the cross-correlation search window aids in constraining the lag times to physically feasible values. The maximum size of the search window is found on the basis of known electronic delays, sensor separation and typical wind speeds, as well as mass flow and tube dimensions of closed-path gas analyzers. In cases where these limits are exceeded, Rebmann et al. (2012) recommend to use the value of the preceding averaging interval.
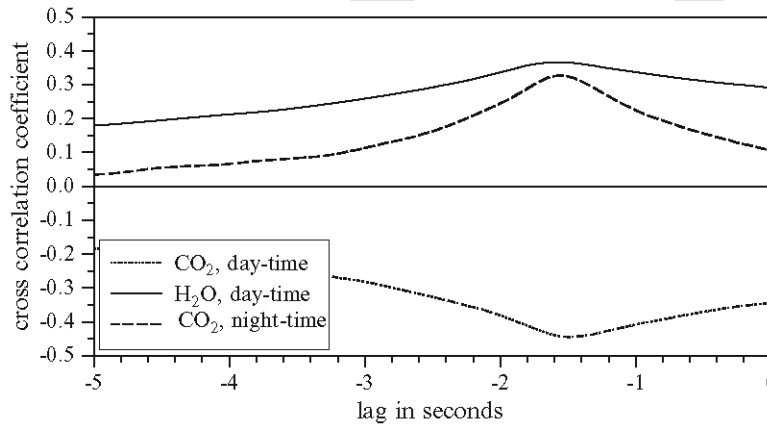
Figure 3. From Rebmann et al. (2012): Cross-correlation between the vertical wind component and CO_2 and H_2O for different lag times.

5.2.1.3   Sonic temperature conversions

The speed of sound in air is not only a function of air temperature, but also of humidity. Hence the temperature measurement by an ultrasonic anemometer/thermometer (SONIC) T_{SONIC} does not equal the air temperature, but includes a cross-dependence on humidity. A conversion is required to cancel this humidity dependence and to yield means, variances and covariances of air temperature T_{air}, respectively (Schotanus et al., 1983);

$$\overline{T_{air}} = \frac{\overline{T_{SONIC}}}{1+0.51\,\overline{FW_{mass,H2O}}}, \tag{4}$$

$$\overline{T_{\text{air}}'^2} = \overline{T_{\text{SONIC}}'^2} - 1.02\, \overline{T_{\text{air}}}\, \overline{T_{\text{air}}' FW_{\text{mass,H2O}}'} - (0.51\, \overline{T_{\text{air}}})^2\, \overline{FW_{\text{mass,H2O}}'^2}, \tag{5}$$

$$\overline{w' T_{\text{air}}'} = \overline{w' T_{\text{SONIC}}'} - 0.51\, \overline{T_{\text{air}}}\, \overline{w' FW_{\text{mass,H2O}}'}, \tag{6}$$

with wet mass fraction (specific humidity) $FW_{\text{mass,H2O}}$. Eqs. (4)–(6) are linear approximations and ignore higher-order terms in their exact definitions. The magnitude of these conversions is in the order of 1–2%, and the accuracy of the approximation for temperature is ≤0.03 K for $0 < FW_{\text{mass,H2O}} < 40$ g kg^{-1} H$_2$O, i.e. better than the accuracy of a sonic thermometer. It can be seen that the conversion of variance and covariance (Eqs. (5)–(6)) are subject to cross-dependence on ambient temperature T_{air} in terms $\overline{T_{\text{air}}}$ and $\overline{T_{\text{air}}' FW_{\text{mass,H2O}}'}$ on the right-hand side. Hence Eqs. (5)–(6) must be solved iteratively, by first substituting T_{air} in respective terms on the right hand side with T_{SONIC}, and subsequently updating T_{air} with the outcomes after each cycle until the results for Eqs. (5)–(6) change by no more than 0.01% between iterations (e.g., Mauder and Foken, 2011). Moreover, T_{SONIC} closely resembles the virtual temperature T_{v}, with a difference in the humidity-related conversion in the order of 0.1%;

$$\overline{T_{\text{air}}} = \frac{\overline{T_{\text{v}}}}{1 + 0.61\, \overline{FW_{\text{mass,H2O}}}}. \tag{7}$$

Consequently, $\overline{w' T_{\text{SONIC}}'}$ is often used as surrogate for the buoyancy flux, e.g. in the computation of the Monin-Obukhov length (AD[03], Rebmann et al., 2012).

5.2.1.4 Calculation of means, variance and standard error

The arithmetic mean of a quantity X (such as wind components u, v, w) with sample size N is calculated as;

$$\bar{X} = \frac{1}{N} \sum_{i=1}^{N} X_i. \tag{8}$$

From here, the sample variance (N−1) and standard deviation of X are calculated;

$$\overline{X'^2} = \frac{1}{N-1} \sum_{i=1}^{N} (X_i - \bar{X})^2, \tag{9}$$

$$\text{std}_{\text{err}}(X) = \sqrt{\overline{X'^2}} / \sqrt{N}. \tag{10}$$

5.2.2 Algorithmic implementation

The EC turbulent exchange data analysis is implemented as part of the eddy4R-Docker EC processing framework (Sect. 3.7), and the algorithmic sequence is summarized in Figure 4.

The calculations described in Sects. 5.2.1.1 – 5.2.1.3 are applied to all data products of product level "dp01 statistics" in Table 1. The process is coded and documented in detail in the R-packages eddy4R.base and eddy4R.qaqc, consisting of the following sequence (incl. function references):

- Calculation is performed individually for datasets of 1 min and 30 min duration.
- De-spiking is performed at native resolution using the eddy4R.qaqc::def.dspk.br86() function.
- Derived variables at native resolution are calculated using the eddy4R.base::wrap.derv.prd.day() function.
- Regression of the planar-fit coefficients is performed using the eddy4R.turb::PFIT_det() function over a moving, centered window of 9 days of 20 Hz data. Data points corresponding to bad sensor diagnostics and spikes are omitted from the regression. The eddy4R.turb::PFIT_apply function is then used to apply the regression coefficients and perform the planar-fit coordinate rotation for the central day of the moving window (day 5).
- Lag-correction is performed at native resolution using the eddy4R.base::def.lag() function.
- Sonic temperature is converted to air temperature.
- Descriptive statistics are calculated using the eddy4R.base::wrap.neon.dp01() function.
- Wavelet-based high-frequency spectral correction is performed on 30-min basis though the following sequence automated in the wrapper function eddy4R.turb::wrap.wave().
  - Periods with missing values >10% are being omitted. For all other periods, < 10% missing values are linearly interpolated.
  - The Waves::cwt() function then uses a Morlet mother Wavelet to perform the continuous Wavelet transform of the 3-D wind components, air temperature, as well as H_2O and CO_2 concentration.
  - In the eddy4R.turb::def.vari.wave() function the cross-scalograms with the vertical wind are calculated, and the absolute spectral power is scale-wise integrated to co-spectra. Then the power-law coefficient in the ISR of the unweighted co-spectrum is regressed in the frequency range 0.1 … 0.5 Hz. In case the coefficient exceeds the range of −1.8 … −1.3, the standard −5/3 power law decay is used. The reference spectral coefficients following the power slope are calculated, and the transfer function against the observed co-spectra is determined in the frequency range >0.5 Hz. The transfer function is then applied directly to the corresponding cross-scalogram. The ratio of the global Wavelet covariance after and before application of the transfer function provides the flux-specific correction factor, which is applied to the classical EC flux Eq. (2).
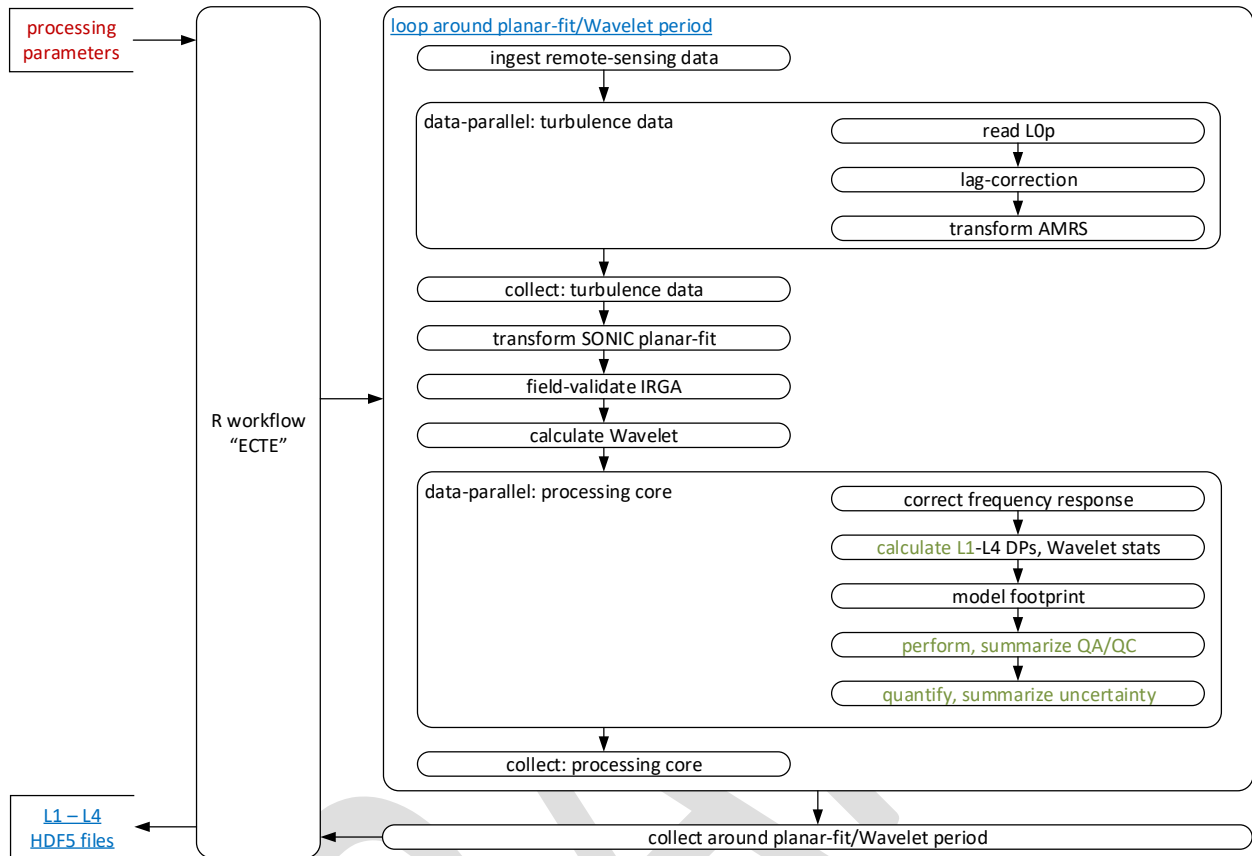
Figure 4. The EC turbulent exchange workflow within the eddy4R-Docker EC processing framework (Sect. 3.7).

5.3 Quality Assurance and Quality Control analysis

Quality flags (*QF*s) are generated for each test and each *QF* can be set to one of three states as shown in Eq. (11) (AD[06]).

$$QF = \begin{cases} 1 \text{ if the quality test failed} \\ 0 \text{ if the quality test passed} \\ -1 \text{ if NA i.e. not able to be run due to a lack of ancillary data} \end{cases} \quad (11)$$

Sensor and statistical QA/QC tests are performed on and reported for the high-frequency data (e.g. 20 Hz), while flux QA/QC tests are reported on time-integrated data per flux averaging period (e.g. 30 min). Here, we utilize the NEON data quality framework as described in AD[06] and Smith et al. (2014) to summarize the results from sensors test and QA/QC tests in a way that is transparent and easily interpretable. In the

following, these sensor health and statistical QA/QC tests are first aggregated to the flux averaging period, and then combined with the results for flux QA/QC tests to determine the QF_{FINAL}.

5.3.1   Theory of Algorithm

A wide range of qualitative and quantitative algorithmic processing routines are applied to EC data products including:

1. Tests related to sensor diagnostics (AD[03]);
2. Statistical plausibility tests, e.g. range, persistence, step (AD[03] and AD[06]);
3. EC-specific tests based on the degree of fulfillment of one or several methodological assumptions, e.g. detection limit, homogeneity and stationarity, development of turbulence tests.

5.3.1.1   Sensor quality flags

Most of quality flags due to the sensor health and statistical plausibility tests are generated as part of the dp0p report variables (AD[03]). In addition, the IRGA validation flag (qfIrgaVali) and *IRGA* automatic gain control quality flag (qfIrgaAgc) were also generated in this ATBD, which are defined below.

1. **IRGA Validation flag** (qfIrgaVali) – is generated to indicate when the sensor is operated under validation period (1 = validation period, 0 = normal operating condition, −1 = NA). The IRGA validation flag is determined from the IRGA sampling mass flow controller flow rate set point as follow:

$$
qfIrgaVali = \begin{cases} 1 \text{ if } frtSet00 = 0 \\ 0 \text{ if } 0.0001333 \leq frtSet00 \leq 0.00025 \\ -1 \; otherwise. \end{cases} \tag{12}
$$

where   frtSet00 is the flow rate set point from IRGA sampling mass flow controller (irgaMfcSamp) in the unit of $m^3 s^{-1}$.

2. ***IRGA automatic gain control quality flag (qfIrgaAgc)*** is indicating when the sensor is operating with low signal strength using 50 percent as the default threshold (1 = when qfIrgaAgc <= 0.50, 0 = when qfIrgaAgc >= 0.50, -1 = NA).

5.3.1.2 Quality budget (QFQM)

The theory of algorithm, the definition of quality flag (*QF*), quality metric (*QM*), alpha (α) and beta (β) *QF*s and *QM*s are detailed in AD[05]. Each of EC DP will have QF_{FINAL}, QM_α, and QM_β associated with it. Aside from QF_{FINAL}, QM_α, and QM_β, each EC DP will also be accompanied by *QM* results for individual tests, representing the fractional occurrence of each state that a quality flag can take.

In order to determine the QF_{FINAL} (Eq. (12)(13)) individually for each DP, the sensor health and statistical plausibility tests are first used to calculate QM_α, and QM_β over the averaging period:

$$QF_{\text{FINAL}} = \begin{cases} 1 & if \ (a \cdot QM_\beta) + (b \cdot QM_\alpha) \geq 20\% \ or \\ & QF_{\text{spec}} \ = \ 1 \ or \\ & QF_{\text{sciRevw}} \ = \ 1 \\ \\ 0 & otherwise \end{cases} \tag{13}$$

where a and b are the ratio of QM_α to QM_β with maximums of 10% for QM_α and 20% for QM_β (more details can be found in AD[05] and (Smith and Metzger, 2013). Therefore, by default a and b are set to 1 and 2, respectively. Then, the results of EC specific (QF_{spec}) tests (i.e., detection limit, homogeneity and stationarity, development of turbulence tests) are taken into account to determine whether the data product is flagged as valid (QF_{FINAL} = 0) or invalid (QF_{FINAL} = 1). If the scientific review flag (QF_{sciRevw}) is set high during science operation management (SOM) review then QF_{FINAL} will be set high.

5.3.2 Algorithmic implementation

The EC turbulent exchange data quality analysis is implemented as part of the eddy4R-Docker EC processing framework (Sect. 3.7), and the algorithmic sequence is summarized in Figure 4.

The calculations described in Sects. 5.3.1.1 – 5.3.1.2 are applied to all data products of product level "dp01 statistics" in Table 1. The process is coded and documented in detail in the R-package eddy4R.qaqc, consisting of the following sequence (incl. function references):

- Calculation is performed individually for datasets of 1 min and 30 min duration.

- Derived quality flags at native resolution for IRGA validation period and AGC are calculated using the eddy4R.qaqc::def.qf.irga.vali and eddy4R.qaqc::def.qf.irga.agc functions, respectively.

- Quality flags are combined into quality metrics using the eddy4R.qaqc::wrap.neon.dp01.qfqm function.

5.4 Uncertainty analysis

5.4.1 Theory of Algorithm

Random errors are defined as the errors due to time averaging over an insufficient period for the time mean to converge to the ensemble mean by the ergodic hypothesis (Lenschow and Stankov, 1986; Lenschow et al., 1994; Lumley and Panofsky, 1964; Mann and Lenschow, 1994).

Here, the random sampling error is estimated using the method of Salesky et al. (2012). In comparison to other available approaches (e.g., Finkelstein and Sims, 2001; Hollinger and Richardson, 2005; Lenschow et al., 1994), the Salesky et al. (2012) method does not require an estimate of the integral time scale or replicate tower measurements. It is also equally applicable to statistical moments of any order, i.e. means, variances and covariance alike. Principally, the method consists of three parts, (i) a local time-series decomposition, (ii) the fitting of a power-law, and (iii) the inter- or extrapolation of the power law.

(i) The high-frequency raw data time-series is low-pass filtered using a running mean filter. This is performed for several filter window sizes $time_{filt}$ in the range 10 $time_{scal} < time_{filt} < time_{agr}$ / 10. Here, $time_{scal}$ is the integral time scale of the process (assumed to be ~1 s), and $time_{agr}$ the duration of the dataset available for aggregation (1,800 s). For each low-pass filtered time-series the standard deviation is calculated as representation of the random error associated with averaging over $time_{filt}$. The random error decreases with increasing window-size of the low-pass filter (Figure 5).

(ii) Next, a power-law in the form of $\sigma = coef_{01}\ time_{filt}^{coef_{02}}$ is regressed to the results (Figure 5). Here, $coef_{01}$ and $coef_{02}$ define the slope and convexity of the uncertainty reduction with increasing window-size of the low-pass filter, respectively. Salesky et al. (2012) relate a value of $coef_{02}$ = −1/2 to the power law decay of random error as derived e.g. by Lenschow et al. (1994) for Gaussian and stationary turbulence. Salesky et al. (2012) restrict their analysis to stationary data and thus permit regression only of $coef_{01}$. In order to also accommodate non-stationary data we additionally permit regression of −1/2 < $coef_{02}$ < 0. It should be noted that for $coef_{02} \rightarrow 0$ the power law becomes less convex, resulting in less uncertainty reduction with increasing window-size. The resulting algorithm such provides a conservative random error estimate for non-stationary data.

(iii) Lastly, $time_{filt}$ in the resulting power law is substituted with the target averaging periods, yielding the corresponding random error.
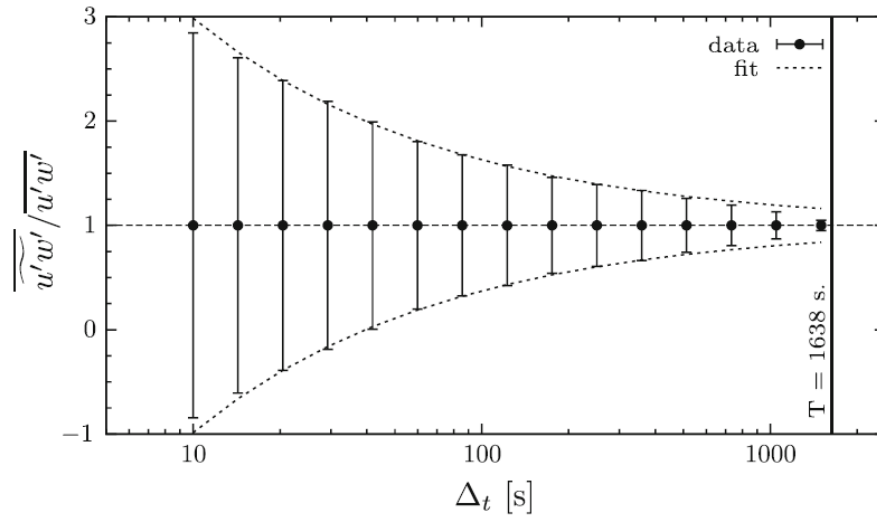
Figure 5. Reduction of standard deviation with increasing window size of the low-pass filter, from Salesky et al. (2012). The error bars denote the standard deviation, and the dashed line denotes a power-law fit.

5.4.2   Algorithmic implementation

The EC turbulent exchange data uncertainty analysis is implemented as part of the eddy4R-Docker EC processing framework (Sect. 3.7), and the algorithmic sequence is summarized in Figure 4.

The random error calculation described in Sect. 5.4.1 is applied to all data products in Table 1. It is coded and documented in detail in the R-function eddy4R.ucrt:: def.ucrt.samp.filt(). In short:

- Calculation is performed individually for datasets of 30 min duration.
- Calculation is only performed if there are less than 10% missing values in the dataset. If less than 10% missing values, those are filled using linear interpolation.
- The signal is de-trended and tapered.
- Filtering is performed using Fast Fourier transform for 10 exponentially spaced filter widths in the range 10 s < $time_{filt}$ < 180 s.
- Nonlinear least squares regression is used to fit the power law.
- The random sampling error is calculated for averaging periods of 1 min and 30 min.

6   STORAGE EXCHANGE

The Eddy Covariance Storage Exchange Assembly (or the EC profile assembly, hereafter referred to as the ECSE) consists of a suite of sensors such as temperature, CO_2 and H_2O gas analyzer and isotopic CO_2 and

H_2O analyzers. The EC profile assembly is served to provide the measurements of temperature, CO_2 and H_2O concentration, the stable isotope of $\delta^{13}C$ in CO_2, $\delta^{18}O$, and $\delta^{2}H$ in water vapor in the atmosphere at each tower measurement level. The vertical profile measurements of temperature, CO_2 and H_2O concentration will be used to calculate the storage fluxes, which will be incorporated into the calculation of the net ecosystem exchange of temperature, CO_2 and H_2O. These DPs are used for constraining, calibrating and validating process-based models (e.g., Rastetter et al., 2010). This shall enable the detection of continental scale ecological change and the forecasting of its impacts.

6.1 Theory of Measurement

6.2 Data Analysis

6.2.1 Theory of Algorithm

The subject of this ATBD is the mathematical derivation of the storage term, $\int_0^{d_{z,m}} \frac{\partial \bar{X}}{\partial t} dz$, in Eq. (1) in Sect. 5.1. It is computed following the steps described below.

6.2.1.1 De-spiking

This part is the same as Sect. 5.2.1.1.

6.2.1.2 Calculation of means, variance and standard error

This part is the same as Sect. 5.2.1.4, but X in the equations refers to temperature, CO_2 concentration and H_2O concentration in ECSE dp01 data product (dp01), instead of turbulent fluxes in ECTE dp01.

6.2.2 Algorithmic implementation

The calculations described in Sect. 6.2.1.1 are applied to generate ECSE dp01 in Table 1. The process is coded and documented in detail in the R-packages eddy4R.base and eddy4R.qaqc, consisting of the following sequence (incl. function references).

6.2.2.1 ECSE dp01

Data flow for signal processing of dp01 IRGA CO_2 concentration (co2Stor) and IRGA H_2O concentration (h2oStor) will be treated in the following order.

- Calculation is performed individually for datasets of 2 min and 30 min duration.

- For each measurement of sampling data, e.g. the data under 000_0n0 folder, the middle two minute data after the first one minute critical time are selected for further calculation, while the critical data are set to be NaN.
- For each measurement of validation data, e.g. the data under co2XXX, the middle two minute before the last 20 s are selected for further calculation, while the last 20 s are set to be NaN.
- De-spiking is performed at native resolution using the eddy4R.qaqc::def.dspk.br86() function.
- Descriptive statistics are calculated using the eddy4R.base::wrap.neon.dp01() function.

6.3   Quality Assurance and Quality Control analysis

The basic quality assurance and quality control analysis can be found in Sect. 5.3. However, sensor and statistical QA/QC tests are performed on and reported for the 1 Hz data for ECSE.

6.3.1   Theory of Algorithm

Details can be found in Sect. 5.3.1.

6.3.1.1   Sensor quality flags

Most of quality flags due to the sensor health and statistical plausibility tests are generated as part of the dp0p report variables (AD[11]).

6.3.1.2   Quality budget (QFQM)

Details of the basic quality budget that applied to ECSE dp01 will be identical to ECTE, which can be found in Sect. 5.3.1.2.

6.3.2   Algorithmic implementation

The calculations described in Sect. 6.2.1.1 are applied to ECSE dp01 in Table 1. The process is coded and documented in detail in the R-packages eddy4R.base and eddy4R.qaqc, consisting of the following sequence (incl. function references).

6.3.2.1   ECSE dp01

Data flow for QA/QC processing of ECSE "dp01 statistics" (dp01) will be treated in the following order.

- Calculation is performed individually for datasets of each duration.
- Using the eddy4R.base::def.idx.agr function to determine the datasets of 2 min and 30 min duration for co2Stor and H2oStor

- Using eddy4R.qaqc::def.neon.dp01.qf.grp function to indicate which quality flags are used as the input variables to determine alpha and beta quality metrics, and final quality flag for each reported dp01.
- Calculated quality metrics, alpha and beta quality metrics, and final quality flag for each reported dp01 using the eddy4R.qaqc::wrap.neon.dp01.qfqm function.

6.4 Uncertainty analysis

6.4.1 Theory of Algorithm

6.4.2 Algorithmic implementation

7 FUTURE PLANS AND MODIFICATIONS

This ATBD currently accounts the algorithmic processing to derive Level 1 (dp01) ECTE and ECSE data products, quality flags and quality metrics, and uncertainty. However, this document is meant to contain all algorithmic processing and subsequent data products derived during the calculation of net surface atmosphere exchange of energy (NEON.DP4.00002, NEON.DP4.00007), water vapor (NEON.DP4.00137), and carbon dioxide (NEON.DP4.00067). Thus, this document will grow as more data products become available.

8 BIBLIOGRAPHY

Baldocchi, D., Finnigan, J., Wilson, K., Paw U, K. T., and Falge, E.: On measuring net ecosystem carbon exchange over tall vegetation on complex terrain, Boundary Layer Meteorol., 96, 257-291, doi:10.1023/a:1002497616547, 2000.

Brock, F. V.: A nonlinear filter to remove impulse noise from meteorological data, J. Atmos. Oceanic Technol., 3, 51-58, doi:10.1175/1520-0426(1986)003<0051:anftri>2.0.co;2, 1986.

Finkelstein, P. L., and Sims, P. F.: Sampling error in eddy correlation flux measurements, J. Geophys. Res. Atmos., 106, 3503-3509, doi:10.1029/2000JD900731, 2001.

Finnigan, J.: A comment on the paper by Lee (1998): "On micrometeorological observations of surface-air exchange over tall vegetation", Agric. For. Meteorol., 97, 55-64, doi:10.1016/s0168-1923(99)00049-0, 1999.

Finnigan, J.: The storage term in eddy flux calculations, Agric. For. Meteorol., 136, 108-113, doi:10.1016/j.agrformet.2004.12.010, 2006.

Finnigan, J. J., Clement, R., Malhi, Y., Leuning, R., and Cleugh, H. A.: A re-evaluation of long-term flux measurement techniques. Part 1: Averaging and coordinate rotation, Boundary Layer Meteorol., 107, 1-48, doi:10.1023/A:1021554900225, 2003.

Foken, T.: Micrometeorology, Springer, Berlin, Heidelberg, 306 pp., 2008.

Foken, T., Leuning, R., Oncley, S. P., Mauder, M., and Aubinet, M.: Corrections and data quality control, in: Eddy covariance: A practical guide to measurement and data analysis, edited by: Aubinet, M., Vesala, T., and Papale, D., Springer, Dordrecht, Heidelberg, London, New York, 85-131, 2012.

Foken, T.: Micrometeorology, 2 ed., Springer, Berlin, Heidelberg, 362 pp., 2017.

Hollinger, D. Y., and Richardson, A. D.: Uncertainty in eddy covariance measurements and its application to physiological models, Tree Physiol., 25, 873-885, doi:10.1093/treephys/25.7.873, 2005.

Kaimal, J. C., and Finnigan, J. J.: Atmospheric boundary layer flows: Their structure and measurement, Oxford University Press, New York, USA, 289 pp., 1994.

Kondo, J., and Sate, T.: The Determination of the von Kármán Constant, Journal of the Meteorological Society of Japan, 60, 461-471, 1982.

Lee, X.: On micrometeorological observations of surface-air exchange over tall vegetation, Agric. For. Meteorol., 91, 39-49, doi:10.1016/s0168-1923(98)00071-9, 1998.

Lee, X., Finnigan, J., and Paw U, K. T.: Coordinate systems and flux bias error, in: Handbook of micrometeorology: A guide for surface flux measurement and analysis, 1 ed., edited by: Lee, X., Law, B., and Massman, W., Springer, Dordrecht, 33-66, 2004.

Lenschow, D. H., and Stankov, B. B.: Length scales in the convective boundary layer, Journal Of The Atmospheric Sciences, 43, 1198-1209, doi:10.1175/1520-0469(1986)043<1198:LSITCB>2.0.CO;2, 1986.

Lenschow, D. H., Mann, J., and Kristensen, L.: How long is long enough when measuring fluxes and other turbulence statistics?, J. Atmos. Oceanic Technol., 11, 661-673, doi:10.1175/1520-0426(1994)011<0661:HLILEW>2.0.CO;2, 1994.

Loescher, H. W., Law, B. E., Mahrt, L., Hollinger, D. Y., Campbell, J., and Wofsy, S. C.: Uncertainties in, and interpretation of, carbon flux estimates using the eddy covariance technique, J. Geophys. Res. Atmos., 111, D21S90-, 2006.

Lumley, J. L., and Panofsky, H. A.: The structure of atmospheric turbulence, Interscience Publishers, New York, 1964.

Mahrt, L., Vickers, D., Howell, J., Højstrup, J., Wilczak, J. M., Edson, J., and Hare, J.: Sea surface drag coefficients in the Risø Air Sea Experiment, J. Geophys. Res., 101, 14327-14335, doi:10.1029/96jc00748, 1996.

Mann, J., and Lenschow, D. H.: Errors in airborne flux measurements, J. Geophys. Res. Atmos., 99, 14519-14526, 1994.

Mauder, M., and Foken, T.: Documentation and instruction manual of the eddy-covariance software package TK3, Universität Bayreuth, Arbeitsergenisse Abteilung Mikrometeorologie, 46, Bayreuth, Germany, 60 pp., ISSN 1614-8924, 2011.

McMillen, R. T.: An eddy correlation technique with extended applicability to non-simple terrain, Boundary Layer Meteorol., 43, 231-245, doi:10.1007/bf00128405, 1988.

Metzger, S., Burba, G., Burns, S. P., Blanken, P. D., Li, J., Luo, H., and Zulueta, R. C.: Optimization of an enclosed gas analyzer sampling system for measuring eddy covariance fluxes of H_2O and CO_2, Atmos. Meas. Tech., 9, 1341-1359, doi:10.5194/amt-9-1341-2016, 2016.

Metzger, S., Durden, D., Sturtevant, C., Luo, H., Pingintha-Durden, N., Sachs, T., Serafimovich, A., Hartmann, J., Li, J., Xu, K., and Desai, A. R.: eddy4R 0.2.0: a DevOps model for community-extensible processing and analysis of eddy-covariance data based on R, Git, Docker, and HDF5, Geosci. Model Dev., 10, 3189-3206, doi:10.5194/gmd-10-3189-2017, 2017.

Nordbo, A., and Katul, G.: A wavelet-based correction method for eddy-covariance high-frequency losses in scalar concentration measurements, Boundary Layer Meteorol., 146, 81-102, doi:10.1007/s10546-012-9759-9, 2012.

Paw U, K. T., Baldocchi, D. D., Meyers, T. P., and Wilson, K. B.: Correction of eddy-covariance measurements incorporating both advective effects and density fluxes, Boundary Layer Meteorol., 97, 487-511, doi:10.1023/a:1002786702909, 2000.

R Core Team: R: A language and environment for statistical computing, R Foundation for Statistical Computing, Vienna, Austria, 2016.

Rastetter, E. B., Williams, M., Griffin, K. L., Kwiatkowski, B. L., Tomasky, G., Potosnak, M. J., Stoy, P. C., Shaver, G. R., Stieglitz, M., Hobbie, J. E., and Kling, G. W.: Processing arctic eddy-flux data using a simple carbon-exchange model embedded in the ensemble Kalman filter, Ecological Applications, 20, 1285-1301, doi:10.1890/09-0876.1, 2010.

Rebmann, C., Kolle, O., Heinesch, B., Queck, R., Ibrom, A., and Aubinet, M.: Data acquisition and flux calculations, in: Eddy covariance: A practical guide to measurement and data analysis, edited by: Aubinet, M., Vesala, T., and Papale, D., Springer, Dordrecht, Heidelberg, London, New York, 59-83, 2012.

Salesky, S., Chamecki, M., and Dias, N.: Estimating the random error in eddy-covariance based fluxes and other turbulence statistics: The filtering method, Boundary Layer Meteorol., 144, 113-135, doi:10.1007/s10546-012-9710-0, 2012.

Schmid, H. P.: Source areas for scalars and scalar fluxes, Boundary Layer Meteorol., 67, 293-318, doi:10.1007/bf00713146, 1994.

Schotanus, P., Nieuwstadt, F. T. M., and Bruin, H. A. R.: Temperature measurement with a sonic anemometer and its application to heat and moisture fluxes, Boundary Layer Meteorol., 26, 81-93, doi:10.1007/BF00164332, 1983.

Smith, D., and Metzger, S.: Algorithm theoretical basis document: Time series automatic despiking for TIS level 1 data products, National Ecological Observatory Network, NEON.DOC.000783, Boulder, U.S.A., 15 pp., 2013.

Starkenburg, D., Metzger, S., Fochesatto, G. J., Alfieri, J. G., Gens, R., Prakash, A., and Cristóbal, J.: Assessment of de-spiking methods for turbulence data in micrometeorology, J. Atmos. Oceanic Technol., 33, 2001 - 2013, doi:10.1175/jtech-d-15-0154.1, 2016.

Stull, R. B.: An Introduction to Boundary Layer Meteorology, Kluwer Academic Publishers, Dordrecht, The Netherlands, 670 pp., 1988.

Tanner, C. B., and Thurtell, G. W.: Anemoclinometer Measurements of Reynolds Stress and Heat Transport in the Atmospheric Surface Layer, University of Wisconsin, Madison, 200, 1969.

Turnipseed, A. A., Anderson, D. E., Blanken, P. D., Baugh, W. M., and Monson, R. K.: Airflows and turbulent flux measurements in mountainous terrain: Part 1. Canopy and local effects, Agric. For. Meteorol., 119, 1-21, doi:10.1016/s0168-1923(03)00136-9, 2003.

Vesala, T., Kljun, N., Rannik, U., Rinne, J., Sogachev, A., Markkanen, T., Sabelfeld, K., Foken, T., and Leclerc, M. Y.: Flux and concentration footprint modelling: State of the art, Environ. Pollut., 152, 653-666, doi:10.1016/j.envpol.2007.06.070, 2008.

Wilczak, J. M., Oncley, S. P., and Stage, S. A.: Sonic anemometer tilt correction algorithms, Boundary Layer Meteorol., 99, 127-150, doi:10.1023/A:1018966204465, 2001.